Journal of Medicinal Chemistry

Article

pubs.acs.org/jmc

# Development of Organometallic S6K1 Inhibitors

Jie Qin,[†,⊥] Rajathees Rajaratnam,[‡,⊥] Li Feng,[‡] Jemilat Salami,[†] Julie S. Barber-Rotenberg,[†,§] John Domsic,[†,§] Patricia Reyes-Uribe,[†] Haiying Liu,[∥] Weiwei Dang,[∥] Shelley L. Berger,[§] Jessie Villanueva,[†] Eric Meggers,*[,‡] and Ronen Marmorstein*[,†,§]

[†]The Wistar Institute, 3601 Spruce Street, Philadelphia, Pennsylvania 19104, United States

[‡]Philipps-Universität Marburg, Hans-Meerwein-Strasse, 35043 Marburg, Germany

[§]Perelman School of Medicine, University of Pennsylvania, 421 Curie Boulevard, Philadelphia, Pennsylvania 19104, United States

[∥]Huffington Center on Aging, Baylor College of Medicine, Houston, Texas 77030, United States

Supporting Information

**ABSTRACT:** Aberrant activation of S6 kinase 1 (S6K1) is found in many diseases, including diabetes, aging, and cancer. We developed ATP competitive organometallic kinase inhibitors, EM5 and FL772, which are inspired by the structure of the pan-kinase inhibitor staurosporine, to specifically inhibit S6K1 using a strategy previously used to target other kinases. Biochemical data demonstrate that EM5 and FL772 inhibit the kinase with $IC_{50}$ value in the low nanomolar range at 100 $\mu$M ATP and that the more potent FL772 compound has a greater than 100-fold specificity over S6K2. The crystal structures of S6K1 bound to staurosporine, EM5, and FL772 reveal that the EM5 and FL772 inhibitors bind in the ATP binding pocket and make S6K1-specific contacts, resulting in changes to the p-loop, $\alpha$C helix, and $\alpha$D helix when compared to the staurosporine-bound structure. Cellular data reveal that FL772 is able to inhibit S6K phosphorylation in yeast cells. Together, these studies demonstrate that potent, selective, and cell permeable S6K1 inhibitors can be prepared and provide a scaffold for future development of S6K inhibitors with possible therapeutic applications.

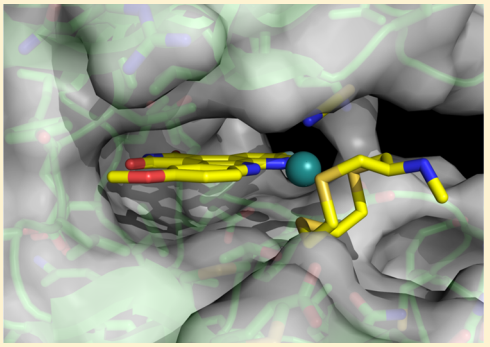

## INTRODUCTION

S6 kinases are members of the AGC serine/threonine kinases of the RSK family, exhibit high homology within their catalytic domain, and are activated by the phosphorylation of a critical residue within the activation loop by phosphoinositide dependent kinase 1 (PDK1). Yeast contains one S6 kinase called Sch9, and humans contain two isoforms called S6K1 and S6K2. S6 kinases act downstream of phosphatidylinositol (3,4,5)-triphosphate ($PIP_3$) in the phosphatidylinositide 3-kinase (PI3K) pathway. Phosphorylation of serine and threonine residues in the C-terminal regulatory domain leads to the phosphorylation of a S6K activation loop residue by PDK1 (residue 252 on the longer splice variant of S6K1).[1] In addition to PDK1, mTOR is also involved in the activation of S6K1[2] and phosphorylates S6K1 at residue T412.

S6 kinases are associated with many cellular processes, including protein synthesis, mRNA processing, cell growth, and cell survival. S6K1 and S6K2 phosphorylate and activate the 40S ribosomal protein S6, which promotes protein synthesis through an increased rate of mRNA transcription.[3] S6K1 also regulates cell size and progression through the cell cycle,[4−6] in addition to promoting cell survival by inactivating the proapoptotic protein BAD.[7]

The aberrant activation of S6 kinases has been shown to play a role in many disease conditions, including diabetes, obesity, aging, and cancer.[8−10] Many melanoma cells harbor constitutive activation of the PI3K-AKT pathway, which results in AKT phosphorylation and leads to activation of the downstream targets mTOR and S6K1.[11] This increase in phosphorylation by S6K1 mediates increased protein translation and cell growth. Treatment with rapamycin, an allosteric mTOR inhibitor, leads to significant dephosphorylation of S6K1 and decreased cell growth.[12] However, treatment with mTOR inhibitors abrogates feedback inhibition of other pathways,[13] which in part leads to side effects such as hyperglycemia, hypercholesterolemia, and hyperlipidemia.[14] Because of this, inhibition of S6K1 represents an alternative therapeutic strategy that may bypass the limitations of mTOR inhibition.

We have previously reported on the development of ATP competitive organometallic kinase inhibitors with high potency and specificity. These inhibitors are structurally inspired by the class of indolocarbazole alkaloids, such as staurosporine, but use a transition metal ion that coordinates up to six ligands to replace the carbohydrate moiety of staurosporine.[15] The scaffold design includes a bidentate ligand that is able to target the metal complexes to the ATP-binding site. This mimics ATP

Special Issue: New Frontiers in Kinases

Received: August 1, 2014
Published: October 30, 2014

   dx.doi.org/10.1021/jm5011868 | J. Med. Chem. 2015, 58, 305−314

and conventional indolocarbazole inhibitors, while the increased size of the bulky transition metal complex allows for exploration of additional chemical space at the edges of the ATP binding site specific to each kinase. Despite being conventional ATP-competitive inhibitors, the combination of unusual globular shape and rigid characteristic of these complexes facilitates the design of highly selective protein kinase inhibitors. It is worth noting that the coordinative bonds to the transition metal are considered to be kinetically stable and are expected to remain intact when exposed to the biological environment, thus avoiding metal-related cytotoxicities.[16−18] However, druglikeness of such complexes, including metabolic stability, bioavailability, and pharmacokinetic properties, is not established yet and is subject to current studies. Regardless, this strategy has led to the development of specific and potent kinase inhibitors for GSK3,[17] PIM1,[19] PI3K,[20] MST1,[21] and BRAF$^{V600E}$.[22]

Here, we present data on the development of potent and specific organometallic S6K1 inhibitors, EM5 and FL772. We show that FL772 binds to S6K1 with an $IC_{50}$ value in the single digit nanomolar range at 100 $\mu$M ATP and that the more potent FL772 compound has a greater than 100-fold specificity over S6K2. Crystal structures of the S6K1 domain bound to the pan-kinase inhibitor staurosporine, EM5, and FL772 reveal that the organometallic inhibitors bind in the ATP binding pocket in a way that is distinct from staurosporine, likely explaining their more favorable potency and selectivity. Cellular data demonstrate that FL772 is able to inhibit S6K phosphorylation in yeast cells. The data provide an important starting point for the development of S6K inhibitors for possible therapeutic applications.

## RESULTS

**Identification of First Generation Organometallic Ruthenium Inhibitors with Potency and Specificity for S6K1.** Inhibitors for S6K1 were initially identified through Millipore KinaseProfiler (Supporting Table 9). Ten different staurosporine-inspired organometallic ruthenium complexes were screened against a diverse panel of 283 protein kinases. This screen led to the identification of EM5 as a potential inhibitor of S6K1, with 7% activity at a concentration of 100 nM in the presence of 10 $\mu$M ATP. EM6, a similar complex replacing the isothiocyanate functional group with an isocyanate (Figure 1A), inhibited significantly less, exhibiting 54% activity under the same conditions. In the kinase panel, the EM5 inhibitor inhibited only 41 kinases (16%) to less than 10% activity, including S6K1 and the related S6K family members RSK1, RSK2, RSK3, and RSK4.

A radioactive kinase assay was used to determine the activity of S6K1 protein constructs prepared in baculovirus-infected insect cells in order to identify a construct that would be suitable for inhibitor testing. Initial tests showed that the full-length $\alpha$I isoform of S6K1 (S6K(1−525)) and the isolated kinase domain (S6K(84−384)) had low kinase activity, although the full-length kinase showed more activity than the kinase domain (Figure 1B). We reasoned that the S6K1 protein constructs had low kinase activity because the full-length kinase contained the C-terminal autoinhibitory domain. To address this issue and express a more active kinase for further inhibitor studies, we prepared a S6K1(1−421) construct including both the T252 and T412 phosphorylation sites, based on previous data from Keshwani et al.[23] indicating that the catalytic domain of the S6K1 aII isoform (residues 1−398) analogous to

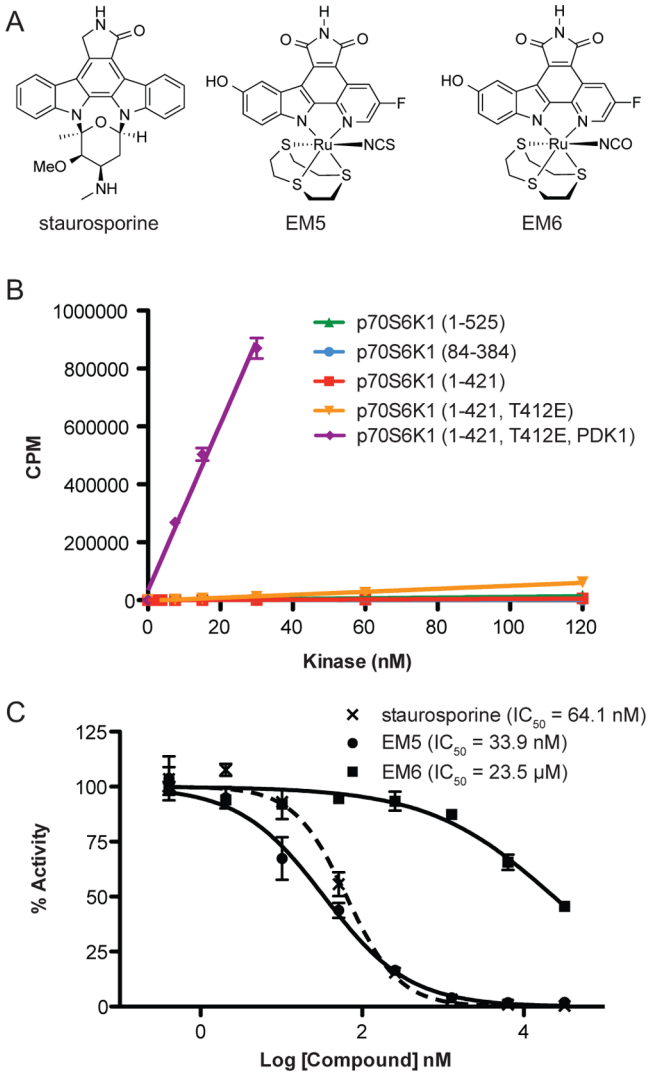


**Figure 1.** First generation organometallic ruthenium inhibitors exhibit potency and specificity for S6K1. (A) EM5 and EM6, two organometallic ruthenium compounds, use a similar structure to mimic the pan-kinase inhibitor, staurosporine. EM6 replaces the isothiocyanate functional group with an isocyanate. (B) A radioactive kinase assay was used to determine the activity of five different protein constructs of S6K1. (C) Staurosporine (dotted line), EM5, and EM6 were assayed against S6K1(1−421, T412E) PDK1 activated in a radioactive kinase assay at 100 $\mu$M ATP. The assay was performed in triplicate.

S6K1(1−421) of the $\alpha$I isoform was highly expressed in insect cells. To further enhance the catalytic activity of S6K1(1−421), we prepared the T412E mutant to mimic phosphorylation at this position and coexpressed the protein with PDK1 to promote phosphorylation of T252. Preparation of the S6K1(1−421, T412E, PDK1 activated) protein resulted in highly active kinase that was suitable for inhibition studies in vitro (Figure 1B).

Both EM5 and EM6 were assayed against S6K1(1−421, T412E, PDK1 activated) in a radioactive kinase assay and determined to have $IC_{50}$ values of 33.9 nM and 23.5 $\mu$M, respectively, at 100 $\mu$M ATP (Figure 1C). For comparison, we also determined the $IC_{50}$ of the nonspecific kinase inhibitor staurosporine, which had an $IC_{50}$ value of 64.1 nM under the same conditions. Given the apparent specificity and potency of


dx.doi.org/10.1021/jm5011868 | J. Med. Chem. 2015, 58, 305−314

Table 1. Data and Refinement Statistics for S6K1 Bound to EM5/Staurosporine and FL772

| | EM5/Stu | FL772 |
|---|---|---|
| resolution range (Å) | 49.03−2.527 (2.618−2.527) | 29.91−2.794 (2.893−2.794) |
| space group | $P12_11$ | $C222_1$ |
| unit cell | | |
| $a$ (Å) | 78.515 | 62.13 |
| $b$ (Å) | 62.882 | 126.371 |
| $c$ (Å) | 86.718 | 110.571 |
| $\alpha$ (deg) | 90 | 90 |
| $\beta$ (deg) | 94.02 | 90 |
| $\gamma$ (deg) | 90 | 90 |
| total reflections | 110 916 | 47 648 |
| unique reflections | 28 440 (2745) | 10 829 (1028) |
| multiplicity | 3.9 (3.3) | 4.4 (4.2) |
| completeness (%) | 99.71 (97.10) | 97.06 (90.33) |
| mean $I/\sigma(I)$ | 21.3 (4.1) | 15.0 (2.0) |
| Wilson $B$-factor | 43.06 | 51.11 |
| $R_{meas}$ (%) | 7.9 (40.7) | 8.9 (67.8) |
| $R_{work}$ (%) | 19.15 (23.61) | 20.63 (29.64) |
| $R_{free}$ (%) | 22.21 (26.70) | 23.01 (32.07) |
| no. of non-H atoms | 4240 | 2114 |
| protein | 4048 | 2040 |
| ligands | 110 | 47 |
| solvent | 82 | 27 |
| rms (bonds (Å)/angles (deg)) | 0.015/1.25 | 0.012/1.03 |
| Ramachandran (% favored/outliers) | 95.0/0 | 95.0/0 |
| average $B$-factor | 40.7 | 55.0 |
| protein | 40.6 | 55.0 |
| ligands | 43.8 | 65.0 |
| solvent | 37.3 | 38.8 |

EM5, it became the lead structure for the development of second-generation organometallic S6K1 inhibitors.

**EM5 Binds to S6K1 in the ATP Binding Pocket in an Unusual Conformation.** Our initial attempts to cocrystallize the S6K1 kinase domain (S6K1KD, residues 84−384) bound to EM5 using several factorial screens were unsuccessful. However, we were able to reproduce the crystals reported by Sunami et al.[24] of the S6K1 kinase domain in complex with staurosporine. We then soaked these crystals with high concentrations of the EM5 inhibitor in the hope of exchanging EM5 for staurosporine in the crystals. The EM5-soaked crystals diffracted to about 2.5 Å resolution and formed in space group $P2_1$ with two molecules per asymmetric unit. The structure was refined to $R_{work}$ and $R_{free}$ values of 19.15% and 22.21%, respectively, with excellent geometry (Table 1). During the refinement process, the inhibitors were modeled only after the protein was fully refined.

Similar to the previously published structures of the S6K1 kinase domain,[24,25] the kinase domain is bilobal, consisting of an N-lobe composed largely of $\beta$-sheet and a C-lobe that is mostly $\alpha$-helical. The crystal structure revealed that one protein molecule in the asymmetric unit was bound to staurosporine, while the other molecule was bound to EM5 in the same ATP binding site. This was confirmed by a $25\sigma$ $F_o - F_c$ difference peak corresponding to the ruthenium atom in the ATP binding sites of one of the molecules before the inhibitor models were built into the electron density map (Figure 2A). This confirms that the EM5 inhibitor is an ATP-competitive inhibitor. The staurosporine and EM5-bound molecules in the asymmetric units are similar to each other with an overall rmsd of 0.68 Å for the shared atoms.

Although both staurosporine and EM5 bind in the ATP binding pocket, the more elaborate EM5 compound makes more extensive interactions, correlating with its greater S6K1 potency than staurosporine. Staurosporine forms hydrogen bonds to S6K1 through the backbone oxygen of Glu-222 of the kinase with the nitrogen of the methylamine of staurosporine, and the backbone nitrogen of Leu-175 and backbone oxygen of Glu-173 of the kinase hinge region contact the pyrrolidone oxygen and nitrogen of staurosporine, respectively. The ring system of staurosporine also makes van der Waals contacts to Leu-97, Lys-99, Gly-98, Val-105, Ala-121, Tyr-174, Glu-179, and Met-225 (Figure 2B).

The EM5 compound retains two hydrogen bonds between the backbone atoms of the hinge residues (Glu-173 and Leu-175) and the maleimide ring of EM5 and all of the van der Waals interactions with the EM5 ring system (Figure 2C). However, in addition to these contacts, EM5 makes additional protein interactions between the ruthenium coordination sphere and the protein. In particular, the additional isothiocyanate group of EM5 makes van der Waals interactions with Gly-100 and Val-105 of the kinase p-loop while the trithiacyclononane ligand makes van der Waals contacts to Gly-100 of the p-loop and Glu-179 and Glu-222 across from the p-loop where the protein substrate is likely to bind and Thr-235 and Asp-236 of the activation loop. Notably, each of these residues (Glu-179, Glu-222, Thr-235, and Asp-236) undergoes a dramatic movement toward the EM5 inhibitor relative to their positions in the staurosporine complex (Figure 2D). The binding of EM5 to S6K1 also introduces significant structural changes in the kinase relative to the staurosporine complex, and these structural changes appear to be indirectly caused by the


dx.doi.org/10.1021/jm5011868 | J. Med. Chem. 2015, 58, 305−314

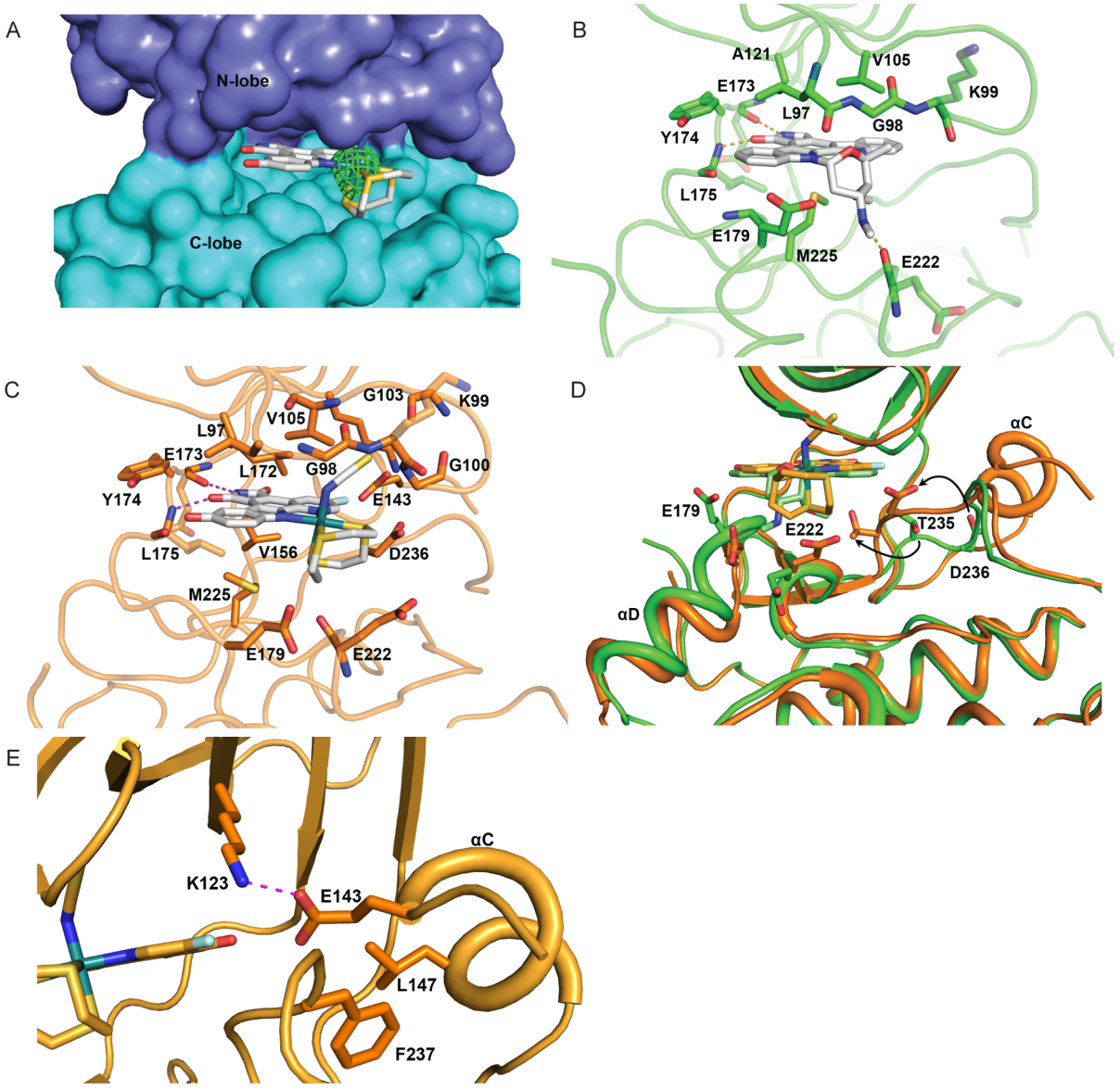


**Figure 2.** EM5 binds to S6K1 in the ATP binding pocket. (A) The electron density map of EM5 (contoured at 12$\sigma$) corresponds to the ruthenium atom of the inhibitor. (B) Interactions between staurosporine and S6K1. Hydrogen bonds are shown as a dashed line, while other interacting residues are labeled. (C) Interactions between EM5 and S6K1. (D) Notable changes between the EM5 and staurosporine bound structures are shown. This includes a change to the activation loop due to EM5 interactions with G100 and V105 and a shortening of two turns to the $\alpha$D helix resulting from an interaction with E179. (E) Close-up around the $\alpha$C helix, which is more ordered in the EM5-bound structure because of an interaction between F237 and L147, and a hydrogen bond between K123 and E143.

1,4,7-trithiacyclononane ligand of the EM5 inhibitor. The $\alpha$D helix of the staurosporine complex is about two turns longer at its N-terminus than the corresponding helix of the EM5 complex where the corresponding segment takes on a $\beta$-strand conformation. This structural difference appears to be driven by the interaction of the tridentate ligand of EM5 with Glu-179.

On the opposite side of the inhibitor, the staurosporine complex contains an activation loop that is folded toward the ATP active site in an inactive conformation and does not have an ordered $\alpha$C helix, as previously reported.[25] Strikingly, the EM5 complex contains a well-defined $\alpha$C helix of about two turns. The difference in disposition of the $\alpha$C helix in the two structures appears to be nucleated around the N-terminal region of the activation loop that undergoes about a 6 Å movement toward the EM5 inhibitor relative to staurosporine. The movement of the activation segment toward the EM5 inhibitor appears to be mediated by the van der Waals interactions that are made between Thr-235 and Asp-236 with the trithiacyclononane ligand of EM5 (Figure 2D). This in turn provides enough room for the $\alpha$C helix to form and to be stabilized by van der Waals interactions between Phe-237 of the activation loop and Leu-147 of the $\alpha$C helix and a hydrogen bonding between Lys-123 of the small domain and Glu-143 of the $\alpha$C helix (Figure 2E). Interestingly, these interactions are characteristic of the active conformations of kinases, even though the activation segment is in an inactive conformation. In contrast, the more out conformation of the activation loop of the staurosporine structure places Phe-237 and Asp-236 in positions that sterically occlude formation of the $\alpha$C helix (Figure 2D). Taken together, while staurosporine binding to S6K1 places it in the inactive conformation, the S6K1/EM5


dx.doi.org/10.1021/jm5011868 | J. Med. Chem. 2015, 58, 305−314

complex has characteristics of both the inactive and active kinase conformations.

**Development of Second-Generation Organometallic Inhibitors.** The EM5 inhibitor bound to S6K1 with an $IC_{50}$ value in the mid-nanomolar range, and a cocrystal structure confirmed that the inhibitor was binding in the ATP pocket of the kinase domain. As a result, EM5 was a promising lead structure for the design of more selective and potent S6K1 inhibitors. Previous data indicate that modifications to the pyridocarbazole moiety or the coordination sphere can have significant effects on binding affinities or kinase selectivity,[26] and the structure of the S6K1/EM5 complex indicated several positions where chemical elaboration could enhance specificity for the kinase. A series of 64 derivatives of EM5 were designed with modifications at the pyridcarbazole heterocycle and the remaining ligand sphere and were tested for inhibition of S6K1 activity using both a radioactive kinase assay (Supporting Information Figure 3A) and an ADP-Glo assay with 1 $\mu$M compound.[27] Twenty-five of these inhibitors were further screened using 250 nM compound (Figure 3A). The eight compounds that inhibited S6K1 to less than 25% activity, the equivalent of EM5, were assayed to determine their $IC_{50}$ values (at 100 $\mu$M ATP). This analysis produced several compounds that inhibited S6K1 similarly or more potently than EM5 including SEK-222 ($IC_{50}$ = 18.9 nM), SEK-243 ($IC_{50}$ = 15.9 nM), SEK-214 ($IC_{50}$= 14.8 nM), SEK-220 ($IC_{50}$= 7.7 nM), and FL772 ($IC_{50}$ =7.3 nM) (Supporting Information Figure 3B). Compound FL772 (Figure 3B) showed the most potent inhibition with an $IC_{50}$ of 7.3 nM, (100 $\mu$M ATP and 2 nM of enzyme) (Figure 3C).

**Characterization of the FL772 S6K1 Inhibitor.** Testing the FL772 inhibitor at a range of concentrations from 1 $\mu$M ATP to 500 $\mu$M ATP resulted in an increase in the $IC_{50}$ value concurrent with increasing ATP concentrations from 3.91 nM at 1 $\mu$M ATP to 25.79 nM at 500 $\mu$M ATP, confirming that FL772 is an ATP competitive inhibitor (Supporting Information Figure 4).[27]

To assess the specificity of FL772 for the S6K1 isoform, we also assayed the FL772 compound against recombinant S6K2 (Figure 3D), which resulted in an $IC_{50}$ value of 975.0 nM, more than 100-fold greater than the $IC_{50}$ value for S6K1. This confirms that the FL772 is indeed specific for the S6K1 isoform over the S6K2 isoform. For comparison, we tested the published S6K1 inhibitor PF-4708671[28] against S6K1 using the radioactive kinase assay in order to compare the potency of our compound with another specific S6K1 inhibitor (Figure 3E). The $IC_{50}$ of PF-4708671 against S6K1 was determined to be 142.8 nM, nearly 20-fold higher than the $IC_{50}$ of FL772 against S6K1.

To establish the kinase selectivity profile of FL772, we submitted the compound at a concentration of 100 nM to the KinomeScan profiling of Lead Hunter Discovery Services using 456 kinases (Supporting Information Table 10). FL772 demonstrated a high degree of kinase selectivity, with only 10 of 456 (2.2%) kinases showing less than 10% activity and only 26 of 456 (5.7%) kinases showing less than 35% activity (Supporting Information Figure 2). Like EM5, FL772 showed binding to the CAM, DAP, FLT, PIM, and RSK family member kinases. Unexpectedly, S6K1 itself exhibited 71% activity in the KinomeScan set of Lead Hunter Discovery Services with 70 of 456 (15.3%) showing a higher degree of binding than S6K1. The potency of FL772 therefore appears to be greater against S6K1 prepared by us than S6K1 prepared by Lead Hunter

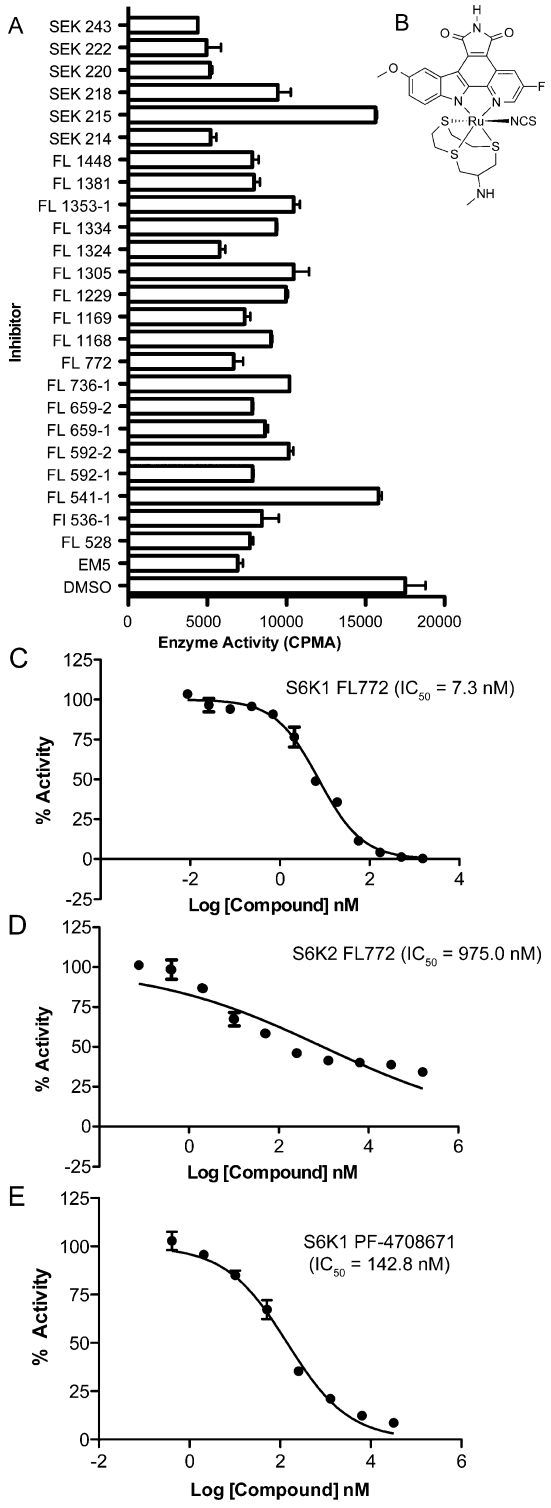


**Figure 3.** Second generation organometallic ruthenium inhibitors have increased potency for S6K1. (A) The 25 top derivatives of EM5 were assayed against S6K1 in a radioactive kinase assay, using 100 $\mu$M ATP and 250 nM S6K1. (B) Structure of the FL772 inhibitor, which showed the most potent inhibition of S6K1. The 1,4,7-trithiacyclononane ligand of EM5 is replaced by a 1,4,7-trithiacyclodecane bearing a methylated amino group in FL772. (C) Radioactive kinase assay of FL772 against S6K1 reveals an $IC_{50}$ of 7.3 nM. (D) Radioactive kinase assay of FL772 against S6K2 shows an $IC_{50}$ of 975 nM. (E) Radioactive kinase assay of PF-4708671 against S6K1 indicates an $IC_{50}$ of 142.8 nM. Panels C, D, and E employed 100 $\mu$M ATP and 2 nM of the respective kinase.


dx.doi.org/10.1021/jm5011868 | J. Med. Chem. 2015, 58, 305−314

Discovery Services. We hypothesize that the different S6K1 kinase preparation and/or phosphorylation state by Lead Hunter Discovery Services leads to the different FL772 potencies for S6K1 measured by us and Lead Hunter Discovery Services. Nonetheless, taking together our analysis of FL772 against S6K1 and the kinase profiling results, we conclude that FL772 exhibits a high degree of kinase selectivity.

FL772 is based on the EM5 lead structure and differs by a methylated hydroxy group at the pyridocarbazole moiety and the thioether-containing tridentate ligand. The nine-membered ring of the symmetrical 1,4,7-trithiacyclononane ligand is replaced by a prochiral 1,4,7-trithiacyclodecane bearing a basic *N*-methylamino group in the 10-membered cyclic tridentate ligand. These structural changes in the tridentate ligand significantly increase the structural complexity of the inhibitor which is exemplified by the number of possible stereoisomers.

To determine the molecular basis for the increased potency of FL772 over EM5, we determined the X-ray crystal structure of FL772 in complex with S6K1 to 2.7 Å resolution (Table 1). The overall structure for the FL772-bound S6K1 is very similar to the EM5-bound structure, with an rmsd of 0.54 Å for all atoms. In particular the p-loop and activation loop and $\alpha$D and $\alpha$C helices take on nearly identical conformations, although the $\alpha$C-helix is about one turn shorter at its N-terminal end (Figure 4A). In addition, the FL772 inhibitor retains all of the interactions made by EM5 but makes some additional interactions including a hydrogen bond between the backbone carbonyl of Lys-99 of the kinase p-loop with the amine ligand of the *N*-methyl-1,4,7-trithiacyclodecan-9-amine ligand while the methyl group makes a van der Waals interaction with Tyr-174 of the kinase hinge region (Figure 4B). These additional interactions of FL772 likely contribute to the greater potency of FL772 over EM5. The protrusion of the amine ligand into the region where protein substrate binds for phosphorylation probably also contributes to the greater inhibitor potency.

**Cellular Properties of FL772.** After establishing that FL772 functions as a potent ATP competitive S6K inhibitor in the in vitro radioactive kinase assay, we carried out studies to characterize its activity in cells. We first tested FL772 for overall cell cytotoxicity and downregulation of phosphorylation of S6 in the 451Lu ($BRAF^{V600E}$ mutant) and 451Lu-MR (BRAF/MEK-inhibitor resistant) melanoma cell lines. Cells were treated with vehicle or a dose of inhibitor ranging from 0.001 to 10 $\mu$M for 22 h (Figure 5A). The 451Lu or 451Lu-MR cell lines exhibited neither a significant decrease in S6 phosphorylation nor a decrease in cell viability as indicated by the absence of cleaved PARP. There was also no change in total S6 or peEF2K levels, indicating that mTOR was not a target of FL772.

We also investigated the effect of FL772 in 293T cells at both 3 and 16 h of treatment (Figure 5B). As controls, we included the compounds AZD8055, PF-4708671, and FL1324. AZD8055 is an ATP-competitive dual mTORC1 and mTORC2 inhibitor that inhibits the phosphorylation of mTORC1 substrates S6K1 and 4EBP1 and the mTORC2 substrate AKT.[29] PF-4708671 is a reported S6K1 inhibitor that does not affect the phosphorylation of AKT. The compound FL1324 is an FL772 analogue identified in our screen that inhibited S6K1 with an $IC_{50}$ of 11 nM (Figure 3A). FL1324 replaces the fluorine of EM5 with a hydroxyl group and is thus a less polar molecule. Since previous studies using PF-4708671 demonstrated a significant reduction in S6 phosphorylation in

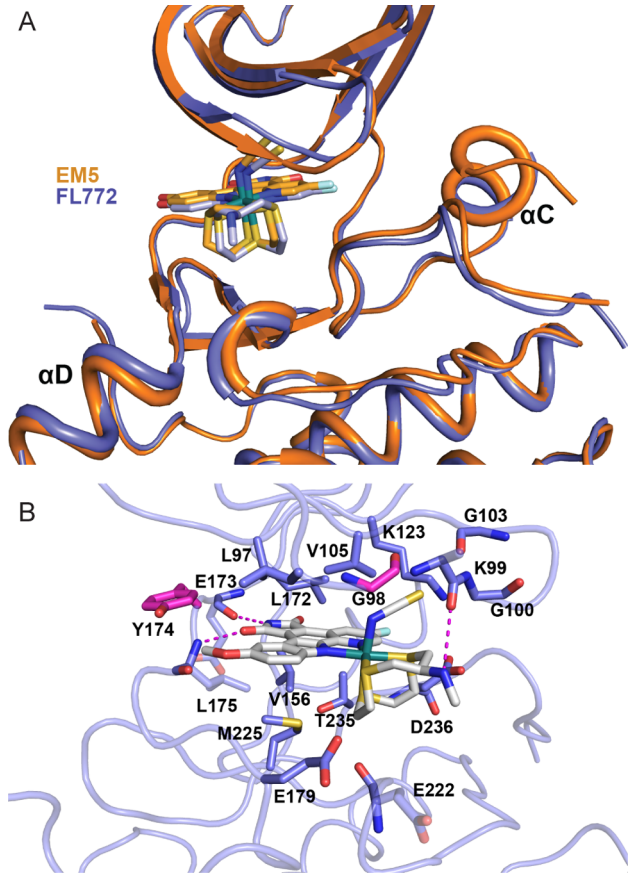


**Figure 4.** FL772 makes complementary interactions with S6K1. (A) Comparison of the S6K1 structures with EM5 and FL772. The $\alpha$C helix of S6K1 is one turn shorter at its N-terminal end of the FL772-bound structure compared to the EM5-bound structure. (B) Interactions between FL772 and S6K1. Hydrogen bonds are shown as a dashed line, while other interacting residues are labeled. FL772-specific interactions that are not made on the EM5-bound structure are highlighted in darker shade. This includes interactions between Y174 and the ether methyl group and the K99 backbone carbonyl with the amine group of the tridentate ligand.

293T cells in 30 min,[28] we tried both a short (3 h) and long (16 h) time point for treatment. As expected, the AZD8055 mTOR inhibitor showed a significant decrease in pS6 levels at both the S235 and S240 sites, along with a decrease in pAKT at T308 and S473. The PF-4708671 compound showed a modest decrease in phosphorylation of S6 at the 3 h time point, but this phosphorylation returned to near basal levels by the 16 h time point. There was no effect on the phosphorylation of AKT. Notably, neither the FL772 nor the FL1324 compound inhibited phosphorylation of S6 or AKT. Together, these results suggest either that the FL772 inhibitor has poor cell membrane permeability or that inhibition of S6K1 in cells does not significantly reduce S6 phosphorylation. The latter possibility is consistent with the fact that the structurally unrelated compound PF-4708671 also shows poor inhibition of S6 phosphorylation in cells and the observation that S6K2 also targets S6 for phosphorylation.[30]

To test if FL772 can inhibit S6 phosphorylation in a setting where S6K2 was not present, we investigated the ability of FL772 to inhibit S6 phosphorylation in budding yeast where a single kinase, Sch9p, is orthologous to human S6K1. We observed that treatment of wild-type budding yeast cells


dx.doi.org/10.1021/jm5011868 | J. Med. Chem. 2015, 58, 305−314

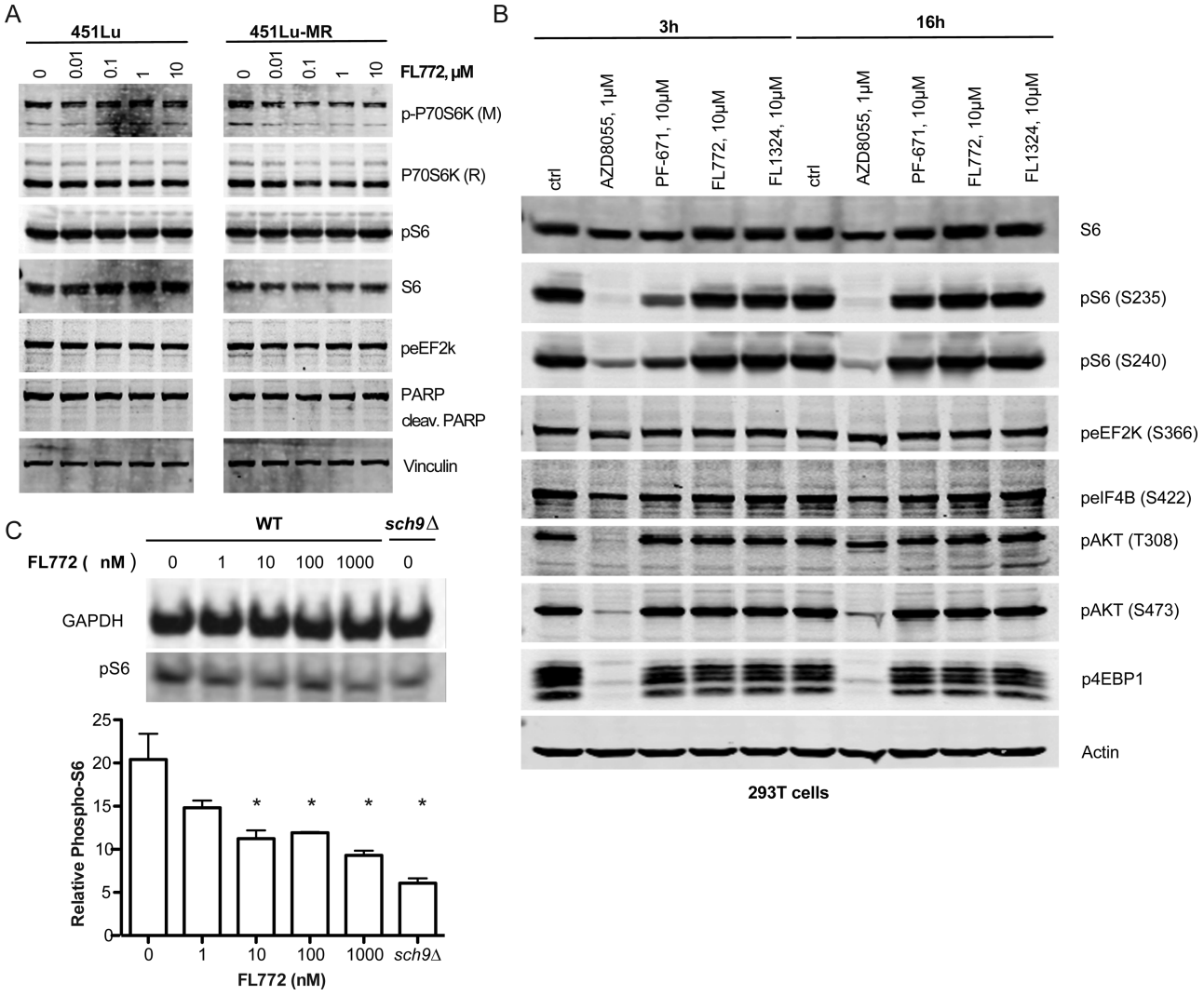


**Figure 5.** FL772 does not inhibit S6 phosphorylation in human melanoma cells but does inhibit S6 phosphorylation in yeast cells. (A, B) Western blot of human cells treated with FL772. (A) 451Lu or 451Lu-MR cells were treated with increasing concentrations of FL772 or vehicle for 22 h. Cells were lysed and blotted for pS6 and other downstream effectors of S6K1. (B) 293T cells were treated with FL772, FL1324 (a similar organometallic ruthenium compound), a previously reported S6K1 inhibitor, PF-671 (4708671), or a previously reported dual mTORC1 and mTORC2 inhibitor, AZD8055, for 3 or 16 h. (C) Western blot of yeast cells treated with FL772. BY4742 budding yeast cells were treated with FL772 for 4 h. Cells were lysed and blotted for pS6. Quantitative Western blot signals were detected by Li-Cor, and the relative pS6 levels were calculated by normalizing raw pS6 measurements to GAPDH signals. (*) $p < 0.05$ (two-tailed Student $t$ test, $n = 3$).

(BY4742) with FL772 significantly decreased the level of phosphorylated S6 in a dose-dependent manner (Figure 5C). At the highest dosage, S6 phosphorylation was reduced to a level similar to the sch9p knockout strain. These data suggest that FL772 functions as an inhibitor of S6 kinases in vivo in a yeast cellular system.

## ■ DISCUSSION AND CONCLUSIONS

In this study, we developed an organometallic ruthenium compound to inhibit S6K1. Using the Millipore KinaseProfiler and radioactive kinase assays, we showed that the EM5 lead compound was a potent and selective S6K1 inhibitor, with 100 nM compound inhibiting 93% of S6K1 activity and only inhibiting 16% of 283 kinases by less than 90%. We found that the EM6 analogue in which an isocyanate group replaces an isothiocyanate is about 1000-fold less potent, implying that potency and specificity could be further optimized. A crystal structure of EM5 bound to S6K1 provided important molecular insights into EM5 inhibition of S6K1 and led to the development of FL772, a compound containing a novel ligand scaffold with an $IC_{50}$ in the single digit nanomolar range for S6K1. A crystal structure of FL772 bound to S6K1 revealed the molecular basis for the compound's potent and selective inhibition of S6K1.

In order to investigate the efficacy of the FL772 inhibitor in cells, we evaluated the inhibitor in both human 293T and $BRAF^{V600E}$ mutant melanoma cells and in budding yeast. We found that FL772 was only able to inhibit S6 phosphorylation in yeast cells, suggesting that either the compound is unable to enter human cells, a significant shift in the $IC_{50}$ of the compound occurs in the presence of physiological levels of ATP, or the uninhibited activity of S6K2 in human cells was sufficient to maintain S6 phosphorylation. Given that ruthenium compounds similar to FL772 have been used to successfully target MST1,[21] PAK1,[31] and PI3K[20] in cells, we do not believe that the ruthenium compounds are unable to


dx.doi.org/10.1021/jm5011868 | J. Med. Chem. 2015, 58, 305−314

penetrate cells. The radioactive kinase assay prohibits measurements at physiological levels of ATP, but we were able to assay the activity of FL772 against S6K1 using an ATP range from 1 to 500 $\mu$M. This analysis revealed that the $IC_{50}$ values increased with increasing ATP concentrations, consistent with FL772 binding competitively with ATP, as also confirmed with the crystal structure of the S6K1/FL772 complex. Interestingly, the $IC_{50}$ ranged from 3.91 nM at 1 $\mu$M ATP to only 25.79 nM (a 6-fold increase) at 500 $\mu$M ATP, suggesting that S6K1 binds ATP relatively loosely and that FL772 is likely to displace ATP even at the higher physiological concentration of ATP. On the basis of these accumulated data, we propose that FL772 is unable to inhibit S6 phosphorylation in human cells because S6 is phosphorylated by the uninhibited S6K2.

S6K1 is closely related to S6K2, sharing 83% sequence identity in the catalytic domain.[32] A study involving S6K1/2 knockdown in mice suggests that both S6K1 and S6K2 are required for full phosphorylation of S6 but that S6K2 may be the more important of the two for phosphorylation of S6.[30] The MEK inhibitor AZD6244 showed additive effects on decreasing the phosphorylation of S6 in vitro when treated in combination with siRNA inhibition of both S6K1 and S6K2 combined, indicating the importance of S6K2 in the phosphorylation of S6.[33] Furthermore, while normal tissues often express low levels of S6K2, overexpression of S6K2 is more common than overexpression of S6K1 in cancer cells.[34−37] Taking these data together suggests that targeting S6K2 either alone or in combination with S6K1 inhibition may be a more viable option for direct S6 inhibition in melanoma and potentially other cancers.

Despite the similarities in the catalytic domain, homology modeling between S6K1 and S6K2 indicates an important difference in residue Tyr-174 that plays an important role in FL772 binding and is a cysteine in S6K2.[38] This residue is located in the hinge region of S6K1 and makes an important van der Waals interaction with the methyl group of the secondary amine, which would not be made with a cysteine residue, suggesting that FL772 may not be a potent inhibitor for S6K2. Indeed, we confirmed in our study that FL772 inhibits S6K2 more than 100-fold more poorly than S6K1. The lethality of $S6K1^{-/-}/S6K2^{-/-}$ knockout mice[30] implies that S6K2 targeting may need to be selective for therapeutic value. To date, there are no commercially available S6K2-selective inhibitors, indicating a potential target for the next series of organometallic ruthenium inhibitors. Taken together, the studies reported here provide a potent and selective S6K1 inhibitor that should be useful to probe S6K1 function and as a starting point for the development of efficacious S6K inhibitors for therapeutic use.

## EXPERIMENTAL SECTION

**Protein Kinase Profiling.** Protein kinase profiling of EM5 was performed with the Millipore KinaseProfiler in a panel of 263 human protein kinases. Percentage of kinase activities were determined for EM5 and EM6 at 100 nM in the presence of 10 $\mu$M ATP. Measurements were performed in duplicate, and the average was taken. Kinase profiling of FL772 was performed with the DiscoveRx Kinome Screen using a panel of 456 kinases. Active-site-directed competition binding was determined in the presence of 100 nM FL772. See the Supporting Information for more details.

**Synthesis of EM5, EM6, and FL772.** EM5 and EM6 were synthesized in analogy to related compounds reported.[39] A detailed synthesis and characterization of FL772 is provided in the Supporting Information.

**Cloning, Expression, and Purification of S6K1 Constructs.** Full length human S6K1 cDNA (1−525) was purchased from Epitope (catalogue number IHS1380-97652397). S6K1 constructs (84−384, 1−421, 1−421 T412E) were subcloned into the pFASTbac HTB vector for protein expression. Sf9 cells were transfected with the recombinant bacmid DNA using Cellfectin (Invitrogen). Cells were harvested after being incubated for 48 h at 28 °C and stored at −80 °C. The 1−421 T412E construct was coexpressed with PDK1 to phosphorylate the T412E residue (cloned from cDNA purchased from OpenBioSystems). Frozen pellets of the S6K1 kinase domain, S6K1(84−384) used for crystallography were resuspended in sonication buffer (50 mM KPi, pH 7.0, 250 mM NaCl, 5% glycerol, 1:1000 PMSF) and sonicated at a power output of 5.5 for 120 s with 20 s intervals (Misonix Sonicator 3000). Lysates were cleared by high-speed centrifugation at 18 000 rpm for 35 min at 4 °C. Equilibrated Talon metal affinity resin (Clontech) was added to cleared lysates and incubated at 4 °C for 1 h with gentle shaking. The resin/lysate mixture was loaded into a gravity flow column, and the resin was extensively washed with wash buffer (50 mM KPi, pH 7.0, 250 mM NaCl, 5% glycerol). Protein was then eluted with elution buffer (50 mM KPi, pH 7.0, 250 mM NaCl, 500 mM imidazole, and 5% glycerol) in a single step. Pooled Talon eluent was diluted 3.5-fold in dilution buffer (50 mM KPi, pH 7.0, 5% glycerol) and loaded onto an SP anion exchange column pre-equilibrated with buffer A (50 mM KPi, pH 7.0, 50 mM NaCl, 5% glycerol). Protein was eluted with buffer B (50 mM KPi, pH 7.0, 500 mM NaCl, 5% glycerol) in a single step. Elution after the Q column was concentrated and loaded to a Superdex s200 column equilibrated with 50 mM Na citrate, pH 6.5, 300 mM NaCl, 1 mM DTT, 5% glycerol. The eluent was collected and concentrated to 3 mg/mL before protein was flash frozen in dry ice and stored at −80 °C. Purification of the 1−421 T412E construct was completed as above, with gel filtration on the Superdex s200 column using a buffer containing 25 mM Tris, pH 7.5, 200 mM NaCl, 1 mM EDTA, and 5% glycerol.

**Cloning, Expression, and Purification of S6K2 Construct.** Full-length human S6K2 cDNA was purchased from GE Healthcare Dharmacon (RPS6KB2, clone identification number 2959036). The S6K2 1−423 construct, equivalent to S6K1 1−421, was subcloned into the pFASTbac HTB vector for protein expression. Sf9 cells were transfected and grown as described above. The construct was coexpressed with PDK1, similar to the S6K1 construct. Frozen pellets were purified identically to the S6K1 1−423 T412E pellets.

**Radioactive Kinase Assay.** Each reaction mixture contained 5 $\mu$L of 5× reaction buffer (100 mM MOPS, pH 7.0, 150 mM $MgCl_2$), 2 $\mu$L of inhibitor in 50% DMSO, 3.6 $\mu$L of S6K1 substrate peptide (RRRLSSLRA), 1 $\mu$L of BSA (20 mg/mL), 3.2 $\mu$L of S6K1 (concentration as described in Results), and 5 $\mu$L of ATP/ATP* mix (concentration as described in Results) in a total reaction volume of 25 $\mu$L. Reaction mixtures were incubated for 1 h at room temperature before being transferred to Whatman paper and washed with 0.75% phosphoric acid. Data were collected using a scintillation counter. All experiments were performed in triplicate. $IC_{50}$ values were determined using sigmoidal dose response with a variable curve in Prism, version 5.

**Crystallization and Structure Determination.** The S6K1 kinase domain crystals were obtained using room temperature hanging drop vapor diffusion by mixing equal volumes of protein (15 mg/mL) preincubated with 1 mM staurosporine with 20−25% (w/v) PEG335, 0.1 M Bis-Tris (pH 5.5−5.7), and 0.2 M $LiSO_4$. Following the growth of crystals, crystal soaking was carried out by incubation with a final inhibitor concentration of 1 mM in cryoprotectant containing the well solution and 15% (w/v) glycerol for 4 h to overnight and flash frozen in liquid nitrogen. Diffraction images were collected at APS beamline 23ID with a 5 $\mu$m microbeam. The structures were determined by molecular replacement using the reported S6K1/staurosporine complex (PDB accession code 3A60) as a search model with the staurosporine removed from the coordinate file and refined with CNS and Coot. The inhibitors were modeled last into the refined structures. Simulated annealing omit maps were employed to unambiguously confirm the modeled inhibitors. For the EM5-soaked crystals, this


dx.doi.org/10.1021/jm5011868 | J. Med. Chem. 2015, 58, 305−314

revealed that one protein molecule in the asymmetric unit was bound to staurosporine while the other protein molecule was bound to EM5. For the FL772-soaked crystals, the asymmetric unit contained a single, domain-swapped monomer and only the FL772 inhibitor was modeled in the binding site. The structures were refined to convergence with a final $R_{work}$ = 19.15% and $R_{free}$ = 22.21% for the S6K1/EM5 structure and a final $R_{work}$ = 20.63% and $R_{free}$ = 23.01% for the S6K1/FL722 structure with excellent geometry (Table 1).

**Cell Culture and Western Blotting.** Human cell lines were cultured in RPMI (10-040-CM; Cellgro) supplemented with 5% fetal bovine serum and harvested at 70% confluence. For immunoblotting, cells were treated for the specified times with the indicated drugs, washed with cold phosphate buffered saline (PBS) containing 100 mM $Na_3VO_4$, and lysed using TNE buffer (150 mM NaCl, 1% (v/v) NP-40, 2 mM EDTA, 50 mM Tris-HCl, pH 8.0) supplemented with protease inhibitors (11697498001; Roche). Proteins were separated by SDS−PAGE and transferred to nitrocellulose membranes (9004700; BioRad). After blocking for 1 h in 5% (wt/vol) dry milk/Tris-buffered saline (TBS)/0.1% (v/v) Tween-20, membranes were incubated overnight at 4 °C with primary antibodies followed by incubation with Alexa Fluor-labeled secondary antibodies (IRDye 680LT goat-anti-mouse or IRDye 800CW goat-anti-rabbit antibodies (LI-COR Biosciences) for 1 h. β-Actin (A5441) and vinculin (V9131) antibodies were obtained from Sigma. p-AKT (4056, 4060), S6 (2317), p-S6 (4858, 5364), S6K1 (2708), p-S6K1 (9234), p-eEF2k (3691), peIF4B (3591), and cleaved PARP (5625) were obtained from Cell Signaling Technologies. Fluorescent images were acquired and by LI-COR Odyssey Imaging System.

**Yeast Cell Culture and Lysis.** Overnight cultures of wild-type yeast cells (BY4742) were diluted in synthetic complete (SC) medium and regrown at 30 °C to early log phase ($OD_{600}$ of 0.2). FL772 was added to an aliquot of culture to the final concentration of 1, 10, 100, and 1000 nM. The treated cultures were further grown at 30 °C for 4 h before harvesting. A culture of *sch9*Δ cells (KS68) was grown and harvested in parallel as a control. Yeast cell pellets were lysed by spinning down cultures at ∼3000 rpm for 3 min at 4 °C, washing with ice-cold water, and broken in lysis buffer as previously described.[40] Whole cell extracts were separated on a 4−12% Bolt gel with MOPS running buffer (Life Technologies), followed by transfer to a PVDF membrane in a Mini Trans-Blot cell (Bio-Rad) at 20 V overnight. The blot was blocked with 3% BSA at room temperature for 2 h and then at 4 °C for 4 h, followed by incubation with primary antibodies, Phospho-S6 (Cell Signaling, catalog no. 2211, 1:1000 dilution), and GAPDH (Thermo, catalog no. MA5-15738, 1:1000 dilution) at 4 °C overnight. Incubation with secondary antibodies (anti-rabbit-DyLight-680 and anti-mouse-DyLight-800, Pierce, 1:10000 dilution) was carried out at room temperature for 1 h before imaging with Li-Cor Odyssey.

## ■ ASSOCIATED CONTENT

### Supporting Information

Two additional figures illustrating the activity of the EM5 analogs against S6K1 and the activity of FL772 at varying ATP concentrations, details on the synthesis of compounds, the crystal structure of the precursor compound of FL772, the structural overview of second generation organometallic S6K1 inhibitors, kinase profiling data for EM5, EM6, and FL772, and additional references. This material is available free of charge via the Internet at http://pubs.acs.org.

### Accession Codes

The coordinates and structure factors for the S6K1/EM5-staurosporine and S6K1/FL772 structures have been deposited into the Protein Data Bank (PDB) under accession numbers 4rlo and 4rlp, respectively.

## ■ AUTHOR INFORMATION


### Corresponding Authors

*E.M.: e-mail, meggers@chemie.uni-marburg.de; phone, 49-6421-2821534.

*R.M.: e-mail, marmor@mail.med.upenn.edu; phone, 215-898-7740.


### Author Contributions

⊥J.Q. and R.R. contributed equally.

J.Q., R.R, L.F., J.S., J.S.B-R., J.D., P.R.-U., H.L., and W.D. performed experiments and analyzed data. R.M. supervised J.Q., J.S., J.S.B.-R., and J.D.; E.M. supervised R.R. and L.F.; J.V. supervised P.R.-U.; S.L.B. supervised W.D.; W.D. supervised H.L.; J.S.B-R., R.R., W.D., E.M., and R.M. analyzed data and wrote the paper; J.S.B-R., J. D., P.R-U., and W.D. prepared the figures. All authors approved the manuscript.

### Notes

The authors declare no competing financial interest.

## ■ ACKNOWLEDGMENTS

This work was supported by U.S. Public Health Service National Institutes of Health Grants PO1 CA025874 (J.V., R.M.) and T32 CA180298 (J.S.B.-R.). We acknowledge support of the Proteomics Core Facility at the Wistar Institute (Grant NIH P30 CA010815) and the University of Pennsylvania DNA Sequencing Facility at the Perelman School of Medicine, University of Pennsylvania (Grant NIH P30 CA016520).

## ■ REFERENCES


(1) Alessi, D. R.; Kozlowski, M. T.; Weng, Q. P.; Morrice, N.; Avruch, J. 3-Phosphoinositide-dependent protein kinase 1 (PDK1) phosphorylates and activates the p70 S6 kinase in vivo and in vitro. *Curr. Biol.* **1998**, *8*, 69−81.

(2) Brown, E. J.; Beal, P. A.; Keith, C. T.; Chen, J.; Shin, T. B.; Schreiber, S. L. Control of p70 s6 kinase by kinase activity of FRAP in vivo. *Nature* **1995**, *377*, 441−446.

(3) Jefferies, H. B.; Fumagalli, S.; Dennis, P. B.; Reinhard, C.; Pearson, R. B.; Thomas, G. Rapamycin suppresses 5′TOP mRNA translation through inhibition of p70s6k. *EMBO J.* **1997**, *16*, 3693−3704.

(4) Chou, M. M.; Blenis, J. The 70 kDa S6 kinase: regulation of a kinase with multiple roles in mitogenic signalling. *Curr. Opin. Cell Biol.* **1995**, *7*, 806−814.

(5) Montagne, J.; Stewart, M. J.; Stocker, H.; Hafen, E.; Kozma, S. C.; Thomas, G. Drosophila S6 kinase: a regulator of cell size. *Science* **1999**, *285*, 2126−2129.

(6) Radimerski, T.; Montagne, J.; Rintelen, F.; Stocker, H.; van der Kaay, J.; Downes, C. P.; Hafen, E.; Thomas, G. dS6K-regulated cell growth is dPKB/dPI(3)K-independent, but requires dPDK1. *Nat. Cell Biol.* **2002**, *4*, 251−255.

(7) Harada, H.; Andersen, J. S.; Mann, M.; Terada, N.; Korsmeyer, S. J. p70S6 kinase signals cell survival as well as growth, inactivating the pro-apoptotic molecule BAD. *Proc. Natl. Acad. Sci. U.S.A.* **2001**, *98*, 9666−9670.

(8) Selman, C.; Tullet, J. M.; Wieser, D.; Irvine, E.; Lingard, S. J.; Choudhury, A. I.; Claret, M.; Al-Qassab, H.; Carmignac, D.; Ramadani, F.; Woods, A.; Robinson, I. C.; Schuster, E.; Batterham, R. L.; Kozma, S. C.; Thomas, G.; Carling, D.; Okkenhaug, K.; Thornton, J. M.; Partridge, L.; Gems, D.; Withers, D. J. Ribosomal protein S6 kinase 1 signaling regulates mammalian life span. *Science* **2009**, *326*, 140−144.

(9) Um, S. H.; Frigerio, F.; Watanabe, M.; Picard, F.; Joaquin, M.; Sticker, M.; Fumagalli, S.; Allegrini, P. R.; Kozma, S. C.; Auwerx, J.; Thomas, G. Absence of S6K1 protects against age- and diet-induced obesity while enhancing insulin sensitivity. *Nature* **2004**, *431*, 200−205.

(10) Barlund, M.; Forozan, F.; Kononen, J.; Bubendorf, L.; Chen, Y.; Bittner, M. L.; Torhorst, J.; Haas, P.; Bucher, C.; Sauter, G.; Kallioniemi, O. P.; Kallioniemi, A. Detecting activation of ribosomal protein S6 kinase by complementary DNA and tissue microarray analysis. *J. Natl. Cancer Inst.* **2000**, *92*, 1252−1259.
(11) Karbowniczek, M.; Spittle, C. S.; Morrison, T.; Wu, H.; Henske, E. P. mTOR is activated in the majority of malignant melanomas. *J. Invest. Dermatol.* **2008**, *128*, 980−987.
(12) Kwon, H. K.; Bae, G. U.; Yoon, J. W.; Kim, Y. K.; Lee, H. Y.; Lee, H. W.; Han, J. W. Constitutive activation of p70S6k in cancer cells. *Arch. Pharmacal Res.* **2002**, *25*, 685−690.
(13) Rodrik-Outmezguine, V. S.; Chandarlapaty, S.; Pagano, N. C.; Poulikakos, P. I.; Scaltriti, M.; Moskatel, E.; Baselga, J.; Guichard, S.; Rosen, N. mTOR kinase inhibition causes feedback-dependent biphasic regulation of AKT signaling. *Cancer Discovery* **2011**, *1*, 248−259.
(14) Rodriguez-Pascual, J.; Cheng, E.; Maroto, P.; Duran, I. Emergent toxicities associated with the use of mTOR inhibitors in patients with advanced renal carcinoma. *Anti-Cancer Drugs* **2010**, *21*, 478−486.
(15) Meggers, E.; Atilla-Gokcumen, G. E.; Bregman, H.; Maksimoska, J.; Mulcahy, S. P.; Pagano, N.; Williams, D. S. Exploring chemical space with organometallics: ruthenium complexes as protein kinase inhibitors. *Synlett* **2007**, 1177−1189.
(16) Smalley, K. S.; Contractor, R.; Haass, N. K.; Kulp, A. N.; Atilla-Gokcumen, G. E.; Williams, D. S.; Bregman, H.; Flaherty, K. T.; Soengas, M. S.; Meggers, E.; Herlyn, M. An organometallic protein kinase inhibitor pharmacologically activates p53 and induces apoptosis in human melanoma cells. *Cancer Res.* **2007**, *67*, 209−217.
(17) Atilla-Gokcumen, G. E.; Williams, D. S.; Bregman, H.; Pagano, N.; Meggers, E. Organometallic compounds with biological activity: a very selective and highly potent cellular inhibitor for glycogen synthase kinase 3. *ChemBioChem* **2006**, *7*, 1443−1450.
(18) Williams, D. S.; Atilla, G. E.; Bregman, H.; Arzoumanian, A.; Klein, P. S.; Meggers, E. Switching on a signaling pathway with an organoruthenium complex. *Angew. Chem., Int. Ed.* **2005**, *44*, 1984−1987.
(19) Bregman, H.; Meggers, E. Ruthenium half-sandwich complexes as protein kinase inhibitors: an *N*-succinimidyl ester for rapid derivatizations of the cyclopentadienyl moiety. *Org. Lett.* **2006**, *8*, 5465−5468.
(20) Xie, P.; Williams, D. S.; Atilla-Gokcumen, G. E.; Milk, L.; Xiao, M.; Smalley, K. S.; Herlyn, M.; Meggers, E.; Marmorstein, R. Structure-based design of an organoruthenium phosphatidyl-inositol-3-kinase inhibitor reveals a switch governing lipid kinase potency and selectivity. *ACS Chem. Biol.* **2008**, *3*, 305−316.
(21) Anand, R.; Maksimoska, J.; Pagano, N.; Wong, E. Y.; Gimotty, P. A.; Diamond, S. L.; Meggers, E.; Marmorstein, R. Toward the development of a potent and selective organoruthenium mammalian sterile 20 kinase inhibitor. *J. Med. Chem.* **2009**, *52*, 1602−1611.
(22) Xie, P.; Streu, C.; Qin, J.; Bregman, H.; Pagano, N.; Meggers, E.; Marmorstein, R. The crystal structure of BRAF in complex with an organoruthenium inhibitor reveals a mechanism for inhibition of an active form of BRAF kinase. *Biochemistry* **2009**, *48*, 5187−5198.
(23) Keshwani, M. M.; Ross, D. B.; Ragan, T. J.; Harris, T. K. Baculovirus-mediated expression, purification, and characterization of a fully activated catalytic kinase domain construct of the 70 kDa 40S ribosomal protein S6 kinase-1 alphaII isoform (S6K1alphaII). *Protein Expression Purif.* **2008**, *58*, 32−41.
(24) Sunami, T.; Byrne, N.; Diehl, R. E.; Funabashi, K.; Hall, D. L.; Ikuta, M.; Patel, S. B.; Shipman, J. M.; Smith, R. F.; Takahashi, I.; Zugay-Murphy, J.; Iwasawa, Y.; Lumb, K. J.; Munshi, S. K.; Sharma, S. Structural basis of human p70 ribosomal S6 kinase-1 regulation by activation loop phosphorylation. *J. Biol. Chem.* **2010**, *285*, 4587−4594.
(25) Wang, J.; Zhong, C.; Wang, F.; Qu, F.; Ding, J. Crystal structures of S6K1 provide insights into the regulation mechanism of S6K1 by the hydrophobic motif. *Biochem. J.* **2013**, *454*, 39−47.
(26) Pagano, N.; Maksimoska, J.; Bregman, H.; Williams, D. S.; Webster, R. D.; Xue, F.; Meggers, E. Ruthenium half-sandwich complexes as protein kinase inhibitors: derivatization of the pyridocarbazole pharmacophore ligand. *Org. Biomol. Chem.* **2007**, *5*, 1218−1227.
(27) Zegzouti, H.; Zdanovskaia, M.; Hsiao, K.; Goueli, S. A. ADP-Glo: a bioluminescent and homogeneous ADP monitoring assay for kinases. *Assay Drug Dev. Technol.* **2009**, *7*, 560−572.
(28) Pearce, L. R.; Alton, G. R.; Richter, D. T.; Kath, J. C.; Lingardo, L.; Chapman, J.; Hwang, C.; Alessi, D. R. Characterization of PF-4708671, a novel and highly specific inhibitor of p70 ribosomal S6 kinase (S6K1). *Biochem. J.* **2010**, *431*, 245−255.
(29) Chresta, C. M.; Davies, B. R.; Hickson, I.; Harding, T.; Cosulich, S.; Critchlow, S. E.; Vincent, J. P.; Ellston, R.; Jones, D.; Sini, P.; James, D.; Howard, Z.; Dudley, P.; Hughes, G.; Smith, L.; Maguire, S.; Hummersone, M.; Malagu, K.; Menear, K.; Jenkins, R.; Jacobsen, M.; Smith, G. C.; Guichard, S.; Pass, M. AZD8055 is a potent, selective, and orally bioavailable ATP-competitive mammalian target of rapamycin kinase inhibitor with in vitro and in vivo antitumor activity. *Cancer Res.* **2010**, *70*, 288−298.
(30) Pende, M.; Um, S. H.; Mieulet, V.; Sticker, M.; Goss, V. L.; Mestan, J.; Mueller, M.; Fumagalli, S.; Kozma, S. C.; Thomas, G. S6K1(−/−)/S6K2(−/−) mice exhibit perinatal lethality and rapamycin-sensitive 5′-terminal oligopyrimidine mRNA translation and reveal a mitogen-activated protein kinase-dependent S6 kinase pathway. *Mol. Cell. Biol.* **2004**, *24*, 3112−3124.
(31) Maksimoska, J.; Feng, L.; Harms, K.; Yi, C.; Kissil, J.; Marmorstein, R.; Meggers, E. Targeting large kinase active site with rigid, bulky octahedral ruthenium complexes. *J. Am. Chem. Soc.* **2008**, *130*, 15764−15765.
(32) Gout, I.; Minami, T.; Hara, K.; Tsujishita, Y.; Filonenko, V.; Waterfield, M. D.; Yonezawa, K. Molecular cloning and characterization of a novel p70 S6 kinase, p70 S6 kinase beta containing a proline-rich region. *J. Biol. Chem.* **1998**, *273*, 30061−30064.
(33) Atefi, M.; von Euw, E.; Attar, N.; Ng, C.; Chu, C.; Guo, D.; Nazarian, R.; Chmielowski, B.; Glaspy, J. A.; Comin-Anduix, B.; Mischel, P. S.; Lo, R. S.; Ribas, A. Reversing melanoma cross-resistance to BRAF and MEK inhibitors by co-targeting the AKT/mTOR pathway. *PLoS One* **2011**, *6*, e28973.
(34) Pardo, O. E.; Wellbrock, C.; Khanzada, U. K.; Aubert, M.; Arozarena, I.; Davidson, S.; Bowen, F.; Parker, P. J.; Filonenko, V. V.; Gout, I. T.; Sebire, N.; Marais, R.; Downward, J.; Seckl, M. J. FGF-2 protects small cell lung cancer cells from apoptosis through a complex involving PKCepsilon, B-Raf and S6K2. *EMBO J.* **2006**, *25*, 3078−3088.
(35) Filonenko, V. V.; Tytarenko, R.; Azatjan, S. K.; Savinska, L. O.; Gaydar, Y. A.; Gout, I. T.; Usenko, V. S.; Lyzogubov, V. V. Immunohistochemical analysis of S6K1 and S6K2 localization in human breast tumors. *Exp. Oncol.* **2004**, *26*, 294−299.
(36) Lyzogubov, V. V.; Lytvyn, D. I.; Dudchenko, T. M.; Lubchenko, N. V.; Pogrybniy, P. V.; Nespryadko, S. V.; Vinnitska, A. B.; Usenko, V. S.; Gout, I. T.; Filonenko, V. V. Immunohistochemical analysis of S6K1 and S6K2 expression in endometrial adenocarcinomas. *Exp. Oncol.* **2004**, *26*, 287−293.
(37) Perez-Tenorio, G.; Karlsson, E.; Waltersson, M. A.; Olsson, B.; Holmlund, B.; Nordenskjold, B.; Fornander, T.; Skoog, L.; Stal, O. Clinical potential of the mTOR targets S6K1 and S6K2 in breast cancer. *Breast Cancer Res. Treat.* **2011**, *128*, 713−723.
(38) Fenton, T. R.; Gout, I. T. Functions and regulation of the 70kDa ribosomal S6 kinases. *Int. J. Biochem. Cell Biol.* **2011**, *43*, 47−59.
(39) Bregman, H.; Carroll, P. J.; Meggers, E. Rapid access to unexplored chemical space by ligand scanning around a ruthenium center: discovery of potent and selective protein kinase inhibitors. *J. Am. Chem. Soc.* **2006**, *128*, 877−884.
(40) Dang, W.; Steffen, K. K.; Perry, R.; Dorsey, J. A.; Johnson, F. B.; Shilatifard, A.; Kaeberlein, M.; Kennedy, B. K.; Berger, S. L. Histone H4 lysine 16 acetylation regulates cellular lifespan. *Nature* **2009**, *459*, 802−807.